Supplementary material for: “Detection and reconstruction of rock glaciers kinematic over 24 years (2000-2024) from Landsat imagery”

Diego Cusicanqui[1], Pascal Lacroix[1], Xavier Bodin[2], Benjamin Aubrey Robson[3], Andreas Kääb[4] and Shelley MacDonell[5,6]

[1]Institut des Sciences de la Terre (ISTerre) CNES, CNRS, IRD, Univ. Grenoble Alpes, Grenoble, 38000, France
[2]Laboratoire EDYTEM, Univ. Savoie Mont-Blanc, Le Bourget du Lac, 73376, France
[3]Department of Earth Science, University of Bergen, Bergen, Norway
[4]Department of Geosciences, University of Oslo, Oslo, 0316, Norway
[5]Centro de Estudios Avanzados en Zonas Áridas (CEAZA), La Serena, Chile
[6]Waterways Centre, University of Canterbury and Lincoln University, Christchurch, New Zealand

Correspondence to: Diego Cusicanqui (diego.cusicanqui@univ-grenoble-alpes.fr)

Table S1. List of medium and high resolution remote sensing data. Light grey cells correspond to the *VHR dataset*. [(a)] Corresponds to those images who have been resampled at a different resolution. [(b)] Vivero et al., 2021, McDonnel et al., 2009; [(c)] Image source from Robson et al., (2021); [(d)] *Bodin X. (unpublished).*

#	Acquisition date	Sensor-type	Raw resolution (m)	Source
1	Mars 31, 2000	Landsat 7	15	USGS (free)
2	May 31, 2000	Aerial	1	Private[(b)]
3	Mars 2, 2001	Landsat 7	15	USGS (free)
4	April 6, 2002	Landsat 7	15	USGS (free)
5	Mars 24, 2003	Landsat 7	15	USGS (free)
6	November 30, 2010	Geoeye	0.5 / 1.0*	AIRBUS/CNES[(c)]
7	Mars 23, 2012	Geoeye	0.7	AIRBUS/CNES[(c)]
8	April 12, 2013	Landsat-8	15	USGS (free)
9	April 15, 2014	Landsat-8	15	USGS (free)
10	November 18, 2014	Pleiades	0.5 / 1.0*	AIRBUS/CNES[(d)]
11	Mars 17, 2015	Landsat-8	15	USGS (free)
12	February 16, 2016	Landsat-8	15	USGS (free)
13	April 23, 2017	Landsat-8	15	USGS (free)
14	Mars 25, 2018	Landsat-8	15	USGS (free)
15	Mars 12, 2019	Landsat-8	15	USGS (free)
16	January 31, 2019	Pleiades	0.5 / 1.0*	AIRBUS/CNES[(c)]
17	Mars 31, 2020	Landsat-8	15	USGS (free)
18	Mars 1, 2020	Pleiades	0.5 / 1.0*	AIRBUS/CNES[(c)]
19	April 24, 2021	Landsat-8	15	USGS (free)
20	April 29, 2022	Landsat-8	15	USGS (free)
21	Mars15, 2023	Landsat-8	15	USGS (free)
22	January 13, 2024	Landsat-8	15	USGS (free)

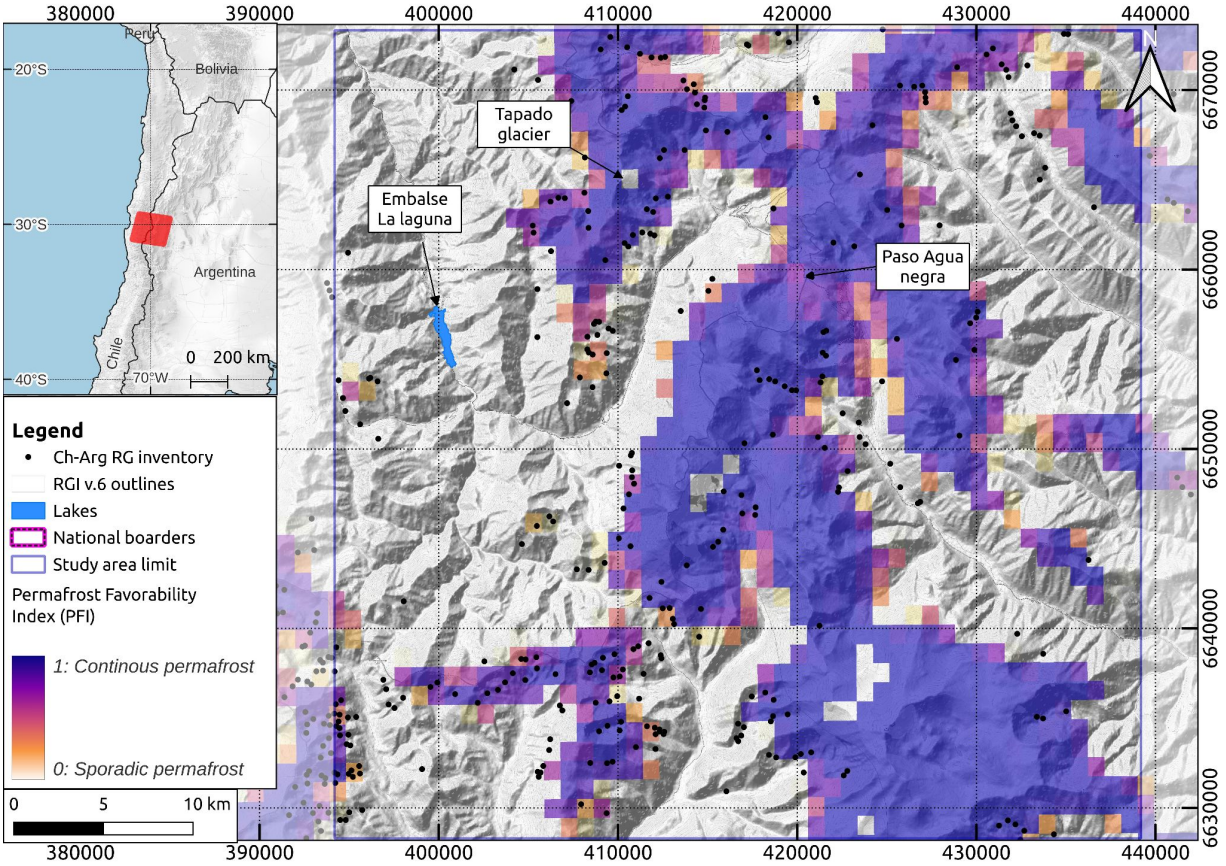

Figure S1. Location of the study area in central dry andes (between 29°20'S and 31°15'S latitude). Red square in the inner map shows the footprint of the Landsat scenes used in this study. Within the main map, black dots correspond to rock glacier inventory for Chile (DGA, 2022) and Argentina (IANIGLA, 2018). The orange-purple colorbar represents the Permafrost Favorability Index (PFI) from (Obu, 2021). Background map corresponds to © OpenTopoMap.

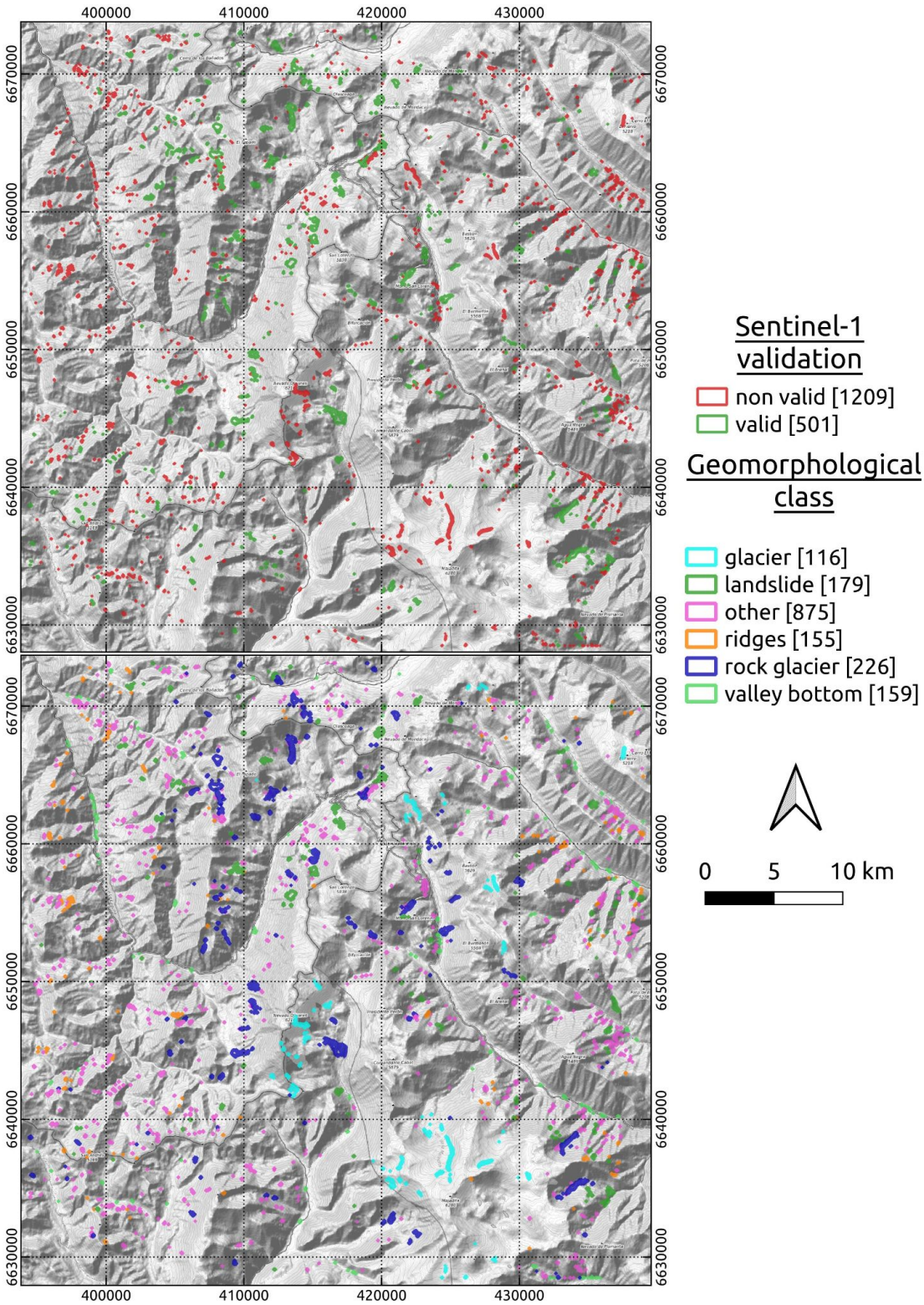

Figure S2. Spatial distribution of raw Persistent Moving Areas (PMA). Upper map shows the comparison of PMA's with InSAR wrapped interferograms. Lower map shows a geomorphological interpretation based on GoogleEarth & Bing high resolution WMS maps.

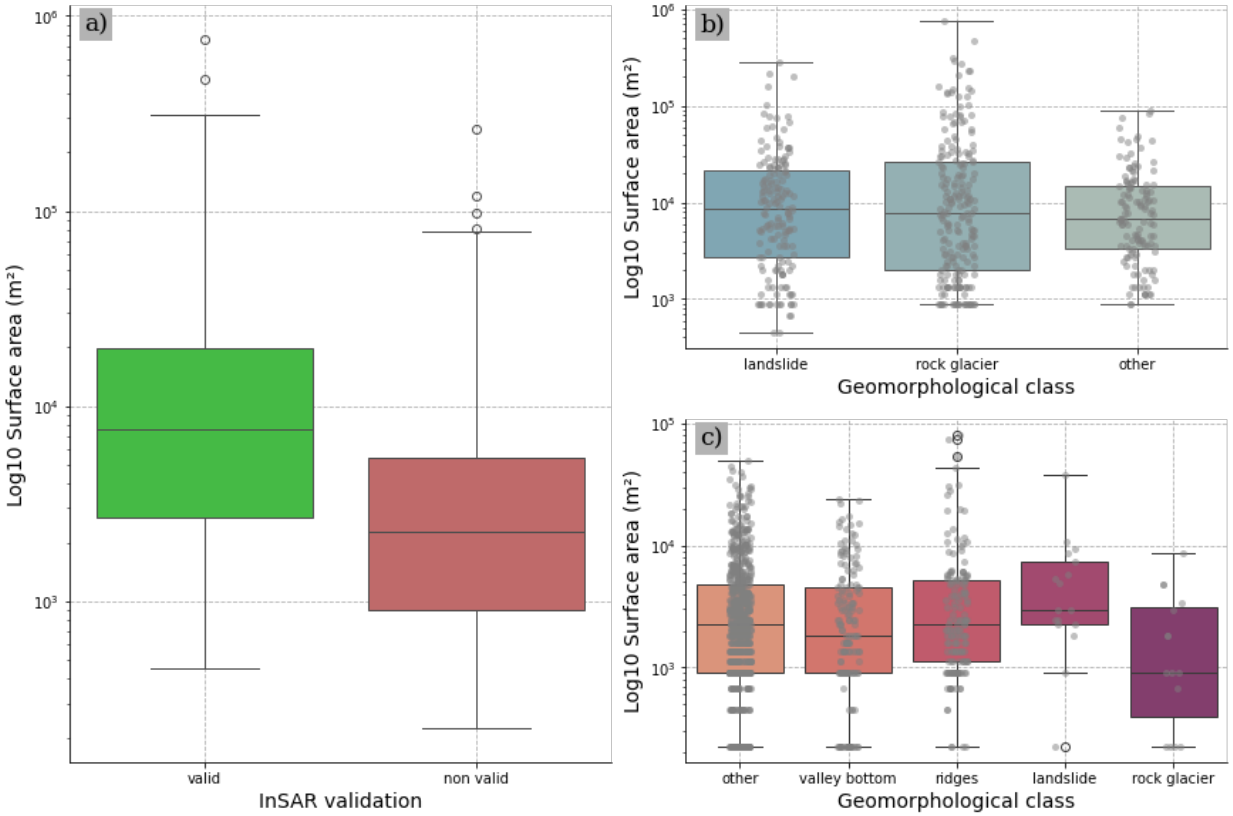

Figure S3. Boxplot representing the distribution of Persistent Moving Areas (PMA) over the study area. a) shows the distribution of valid and non-valid polygons obtained though the S1-and geomorphological validation; b) and c) shows the distribution of valid and non-valid polygons and their respective geomorphological class.

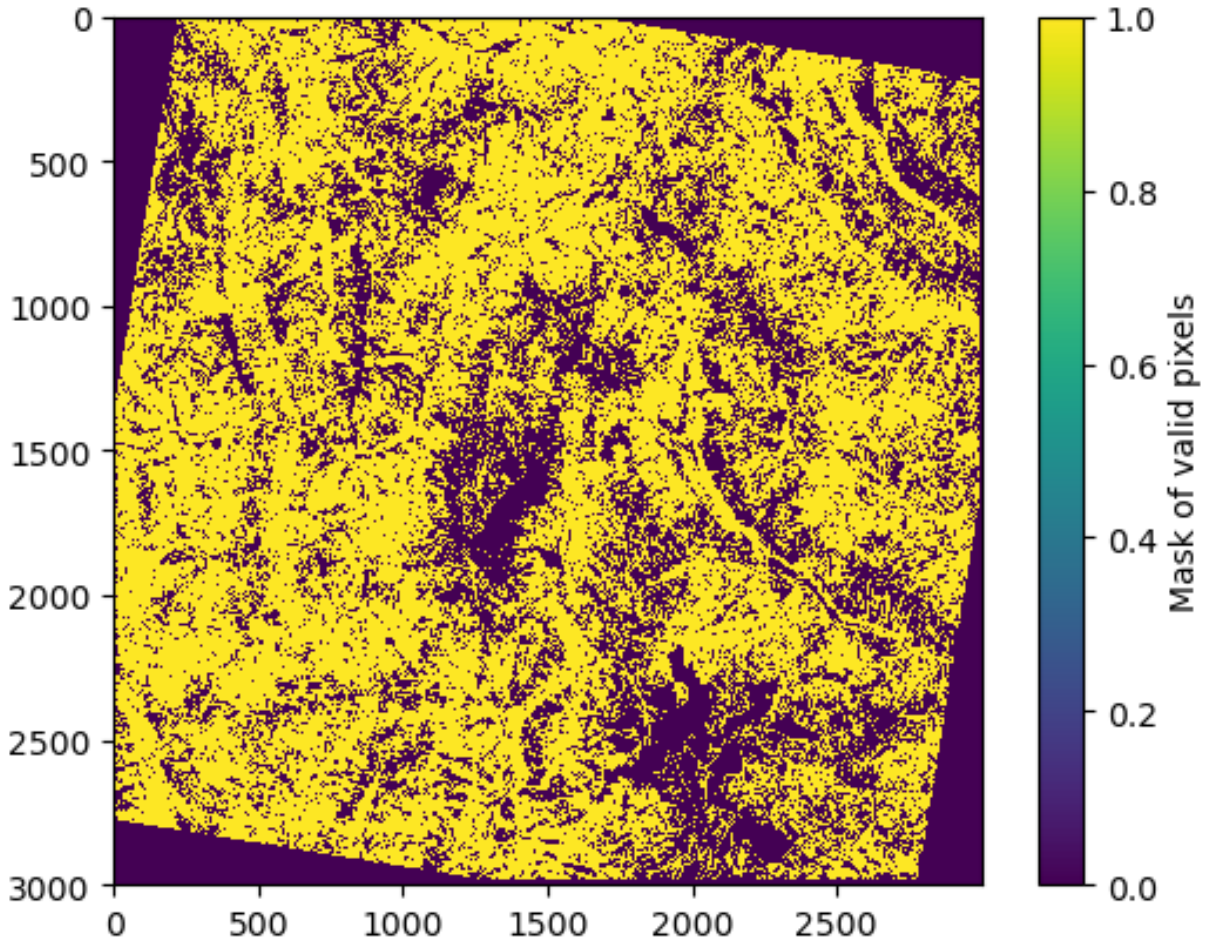

Figure S4. Mask of valid pixels used as stable areas for surface velocity uncertainty computation. For this mask, we removed slopes > 35°, glaciers and PMA outlines. The total amount of valid pixels is 5500117, corresponding to 60% of the entire image footprint.

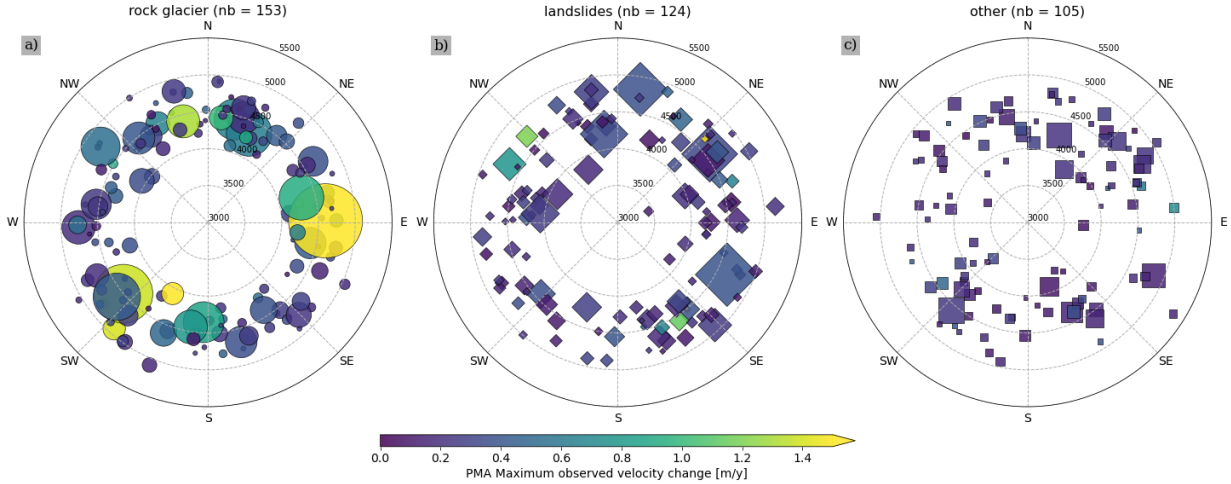

Figure S5. Distribution of PMA ranged by elevation and slope orientation: a) rock glaciers, b) landslides, c) others. Colorbar represents the Top 50% mean velocity for each PMA.

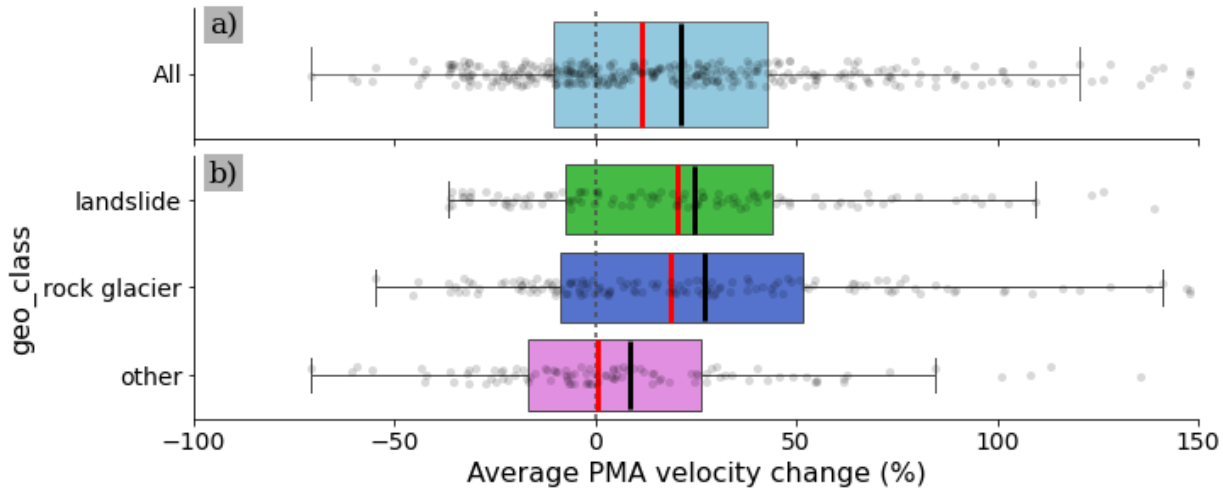

Figure S6. Boxplot showing average percentage of velocity change by PMA for the periods 2000-2014 and 2013-2024. Upper boxplot shows the distribution of the all PMA's. Lower boxplot show the distribution of PMA ordered by geomorphological classification. Red and black lies represents the median and average for each dataset, respectively.

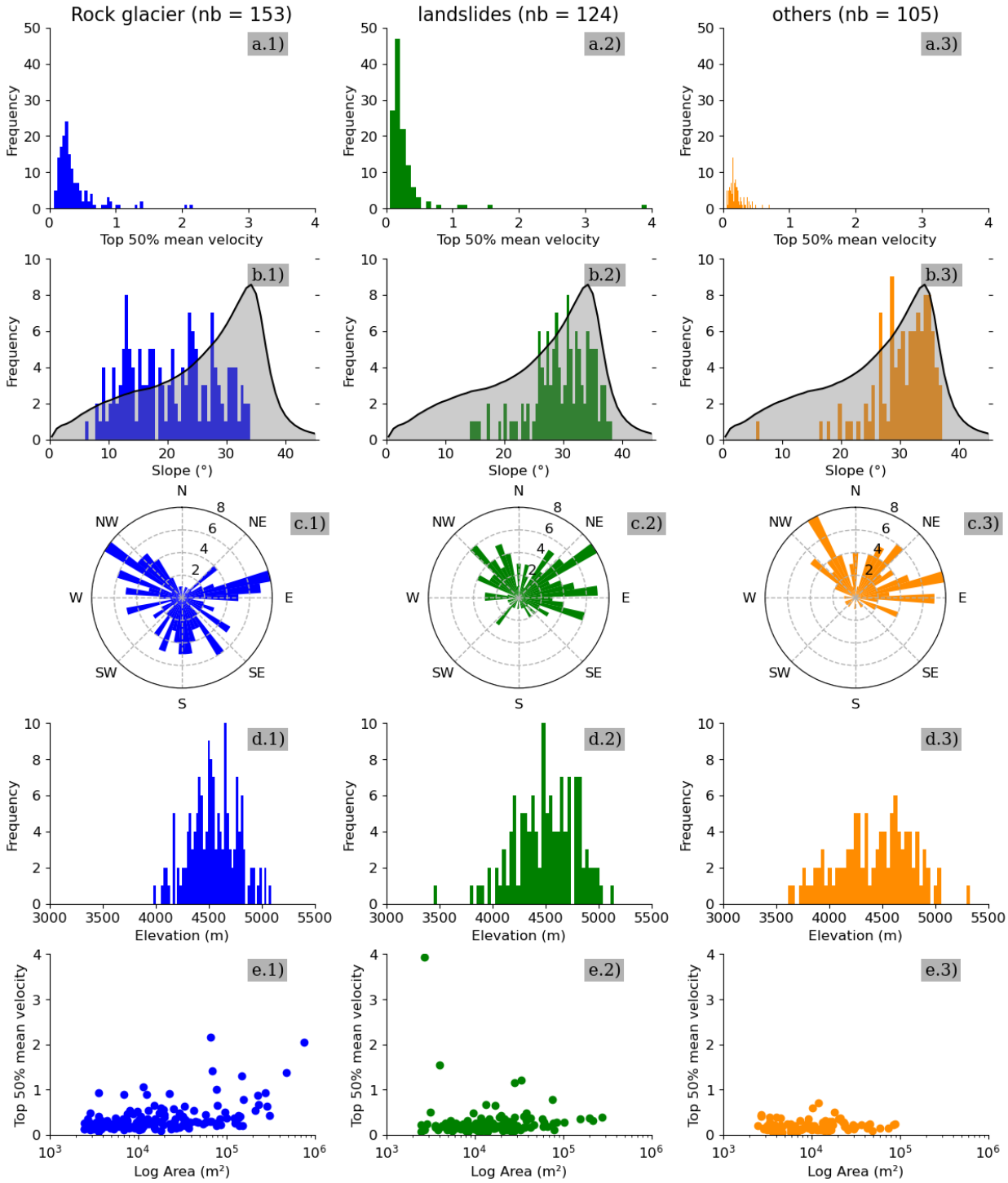

Figure S7. Comparison of the PMA distribution for rock glacier, landslides and other geomorphological class vs topographical context. a) Top 50% mean velocity; b) mean slope; c) slope orientation; d) elevation and e) distribution between Top 50% mean velocity PMA surface.

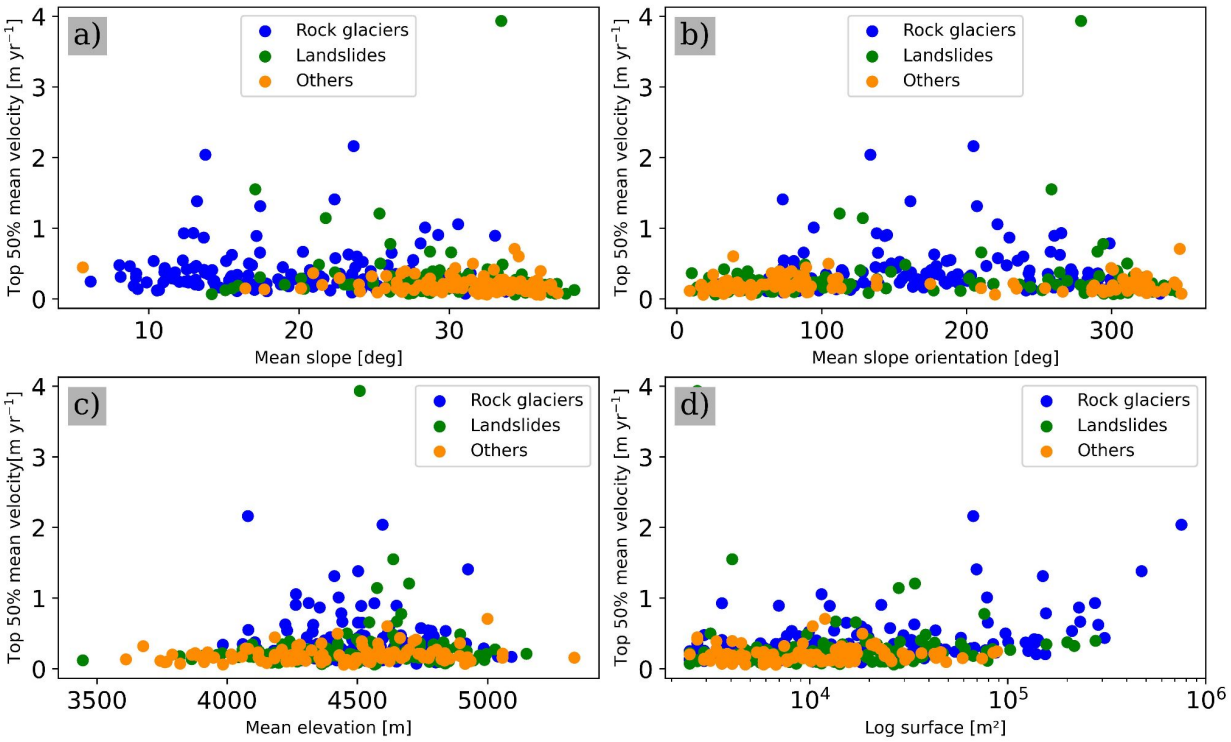

Figure S8. Comparison of the Top 50% mean velocity for each PMA for rock glacier, landslides and other geomorphological class vs topographical context. a) mean slope; b) slope orientation; c) elevation and d) PMA surface.

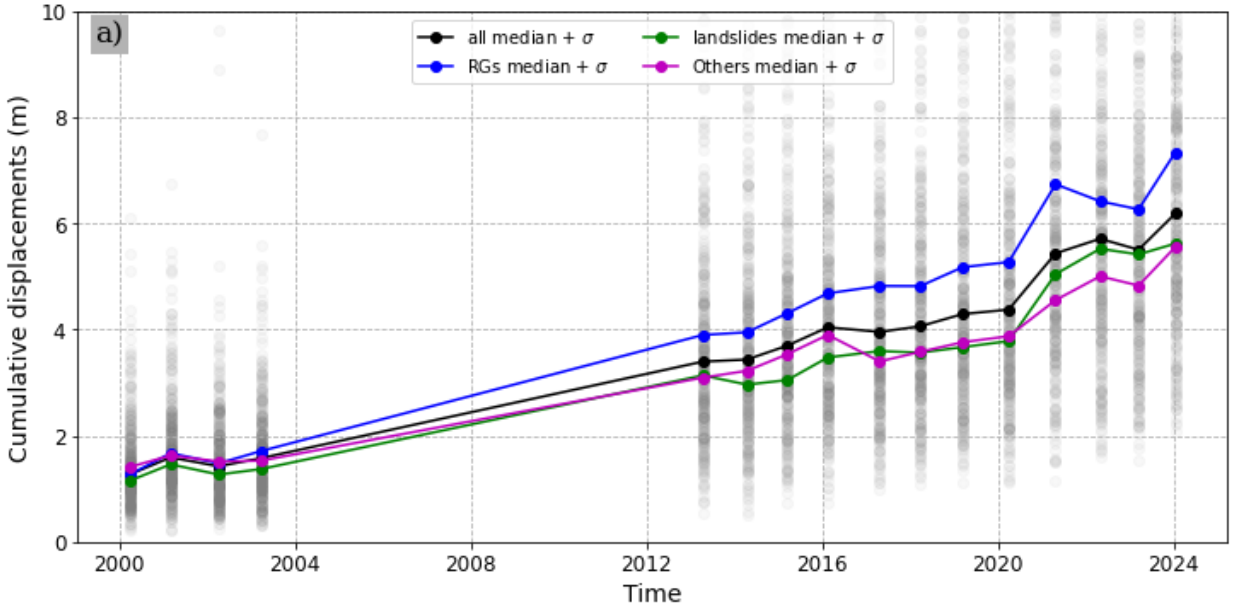

Figure S9. Time series of displacements for all filtered PMA. Grey dots shows the top 50% median surface velocity for each PMA. Blue, green, magenta and black dots and lines, shown the top 50% median surface velocity for each class (rock glaciers, landslide, others and all PMA dataset, respectively).

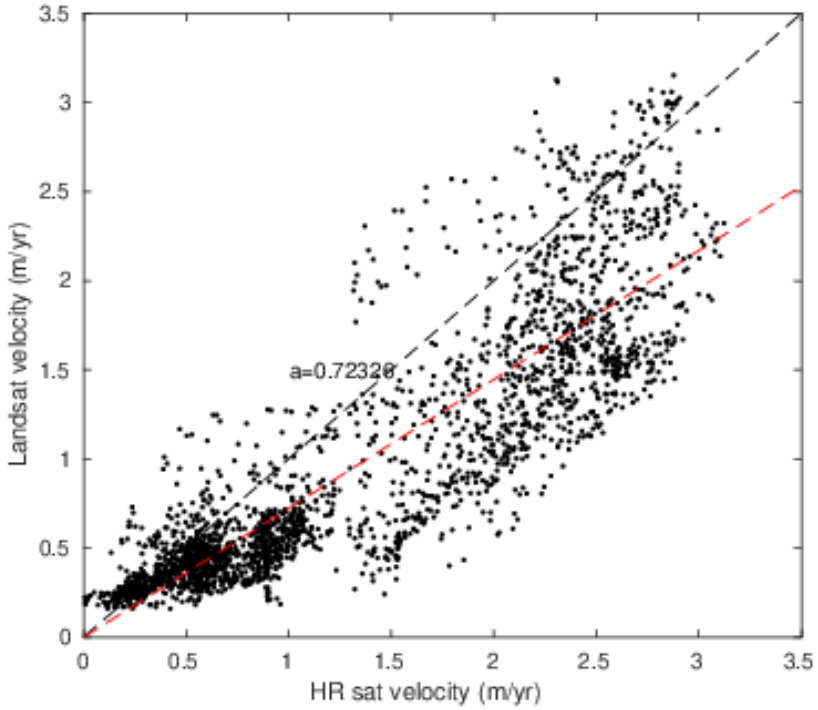

Figure S10. Pixel-to-pixel comparison of both HR dataset xs L7/8 dataset over Tapado complex area and largo rock glacier.

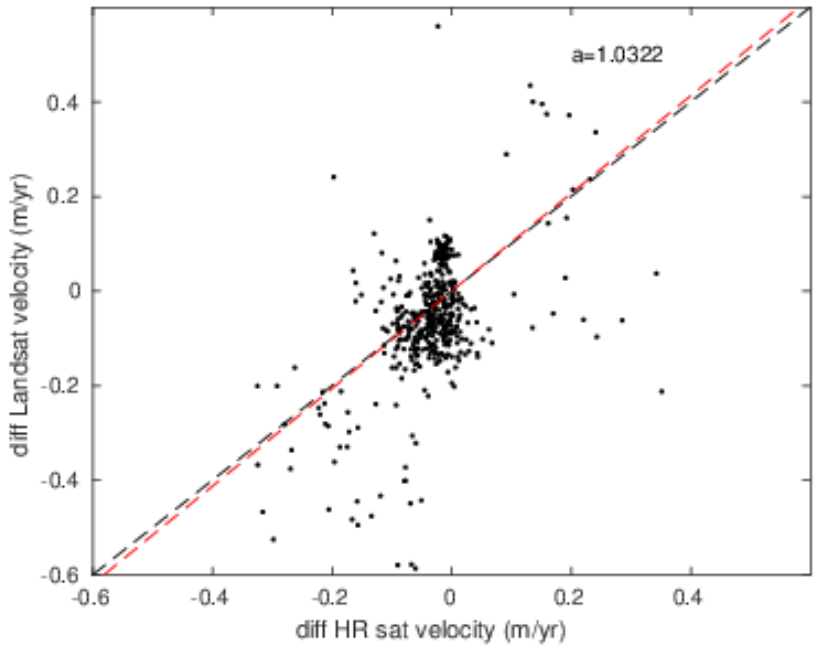

Figure S11. Changes in velocity between two periods 2000 - 2013 & 2013 - 2024.

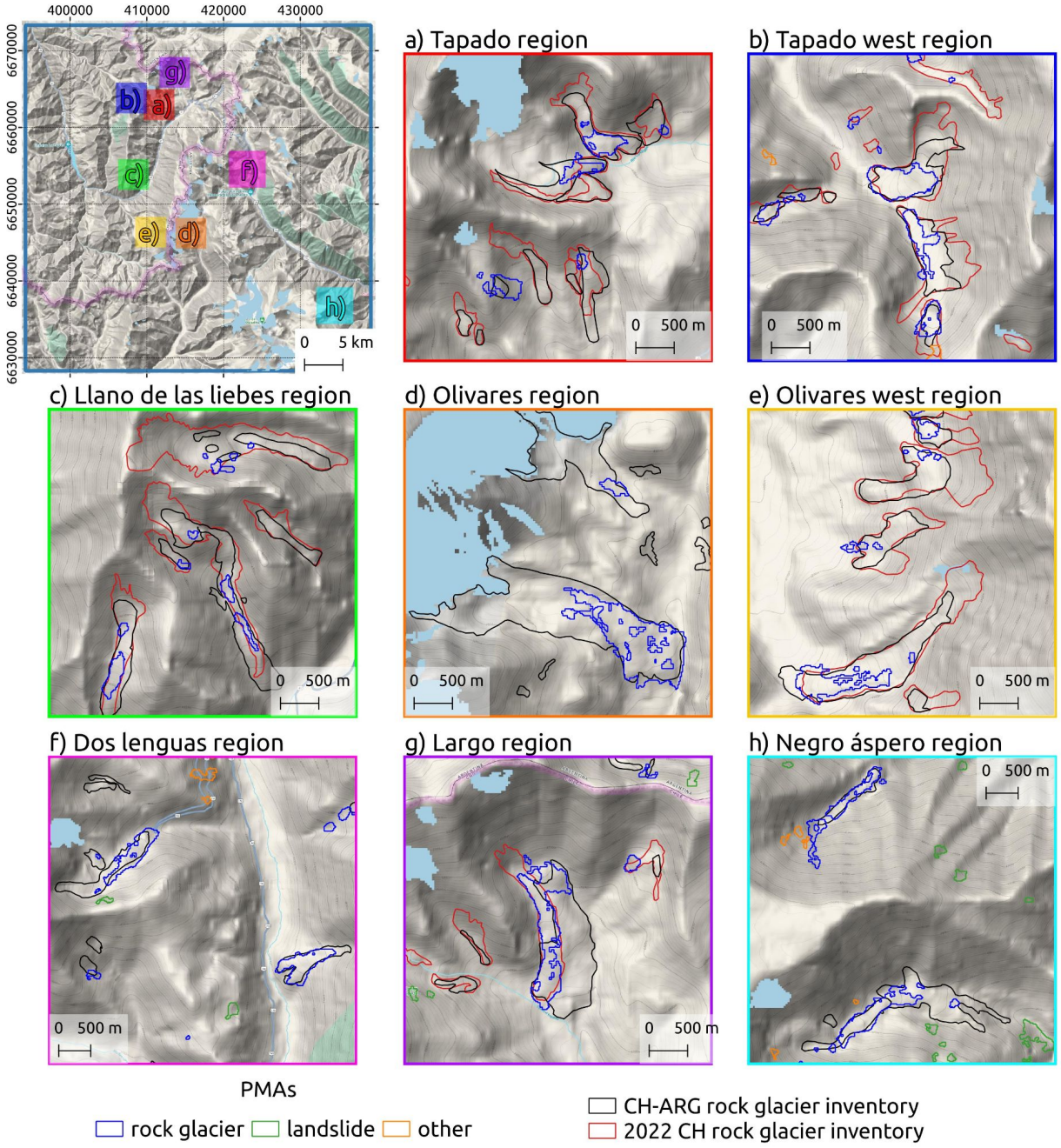

Figure S12. Comparison between existing rock glacier inventories and PMA detection. Black polygons represent Chile and Argentina 2013 (DGA, 2013) and 2018 (IANIGLA, 2018) rock glacier outlines.Red polygons shows the updated version of the rock glacier inventory for Chile (DGA, 2022).

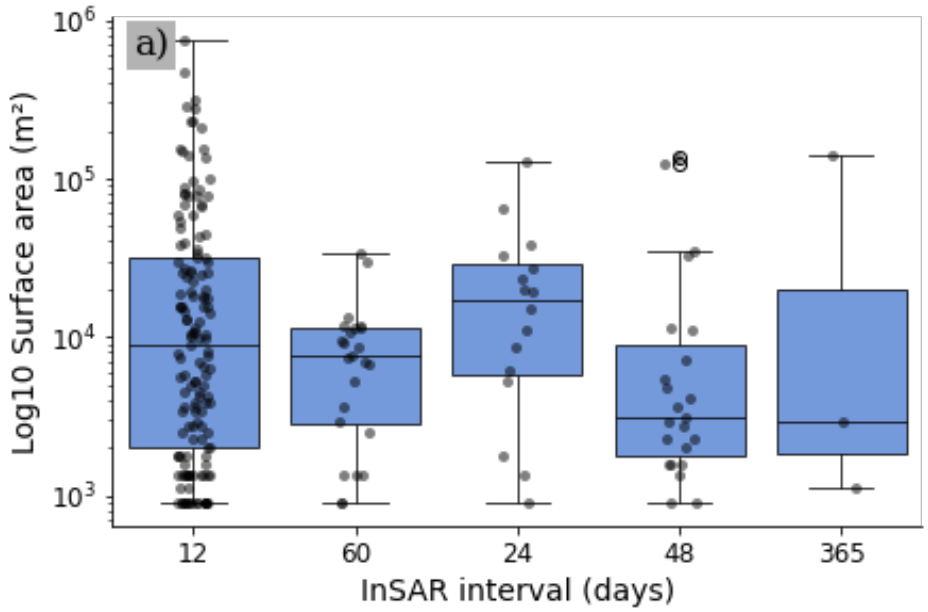

Figure S13. The box plot shows the surface distribution of PMAs ordered by the number of days of the interferograms on where the PMA is also detected.

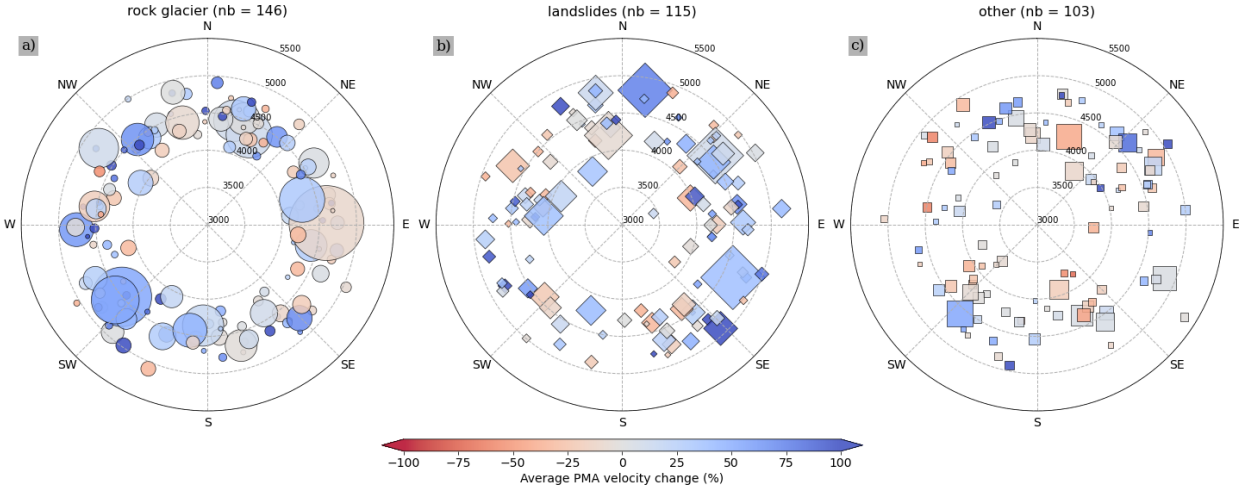

Figure S14. Polar plot showing the distribution of each PMA ordered by geomorphological class. Points are ordered by slope orientation and 500m altitudinal bins. Colorbar show the percentage of velocity change and size of symbol represents the PMA surface.